Early stage ettringite and monosulfoaluminate carbonation investigated by in situ Raman spectroscopy coupled with principal component analysis

Mohamed-Nadjib Brahim, Jean-Michel Mechling, Sarah Janvier-Badosa, Mario Marchetti

Early stage ettringite and monosulfoaluminate carbonation investigated by *in situ* Raman spectroscopy coupled with principal component analysis

Brahim Mohamed-Nadjib, Mechling Jean-Michel, Janvier-Badosa Sarah, Marchetti Mario

PII: S2352-4928(23)00229-5

DOI: https://doi.org/10.1016/j.mtcomm.2023.105539

Reference: MTCOMM105539

To appear in: *Materials Today Communications*

Received date: 6 October 2022
Revised date: 21 December 2022
Accepted date: 1 February 2023

Please cite this article as: Brahim Mohamed-Nadjib, Mechling Jean-Michel, Janvier-Badosa Sarah and Marchetti Mario, Early stage ettringite and monosulfoaluminate carbonation investigated by *in situ* Raman spectroscopy coupled with principal component analysis, *Materials Today Communications,* (2022) doi:https://doi.org/10.1016/j.mtcomm.2023.105539

Early stage ettringite and monosulfoaluminate carbonation investigated by *in situ* Raman spectroscopy coupled with principal component analysis

Brahim Mohamed-Nadjib[a,*], Mechling Jean-Michel[a], Janvier-Badosa Sarah[a], Marchetti Mario[a,b]

[a] Université de Lorraine, CNRS, IJL, F-54000 Nancy, France

[b] Université Gustave Eiffel, MAST, FM2D, IFSTTAR, 14-20 Boulevard Newton, cité Descartes, Champs sur Marne, F-77447 Marne la Vallée Cedex 2, France

Abstract

This study investigates the early stages of monosulfoaluminate and ettringite carbonation using non-destructive *in situ* Raman spectroscopy monitoring. Coupling this technique with Principal Components Analysis enables relevant information to be extracted from spectral data such as an accurate identification of the beginning of the reaction and of specific chemical phases. These two hydrates and some of their carbonation products can be well detected using this vibrational spectroscopy technique. Experiments were conducted on two pastes of hydrated yeelimite, in the presence and in the absence of gypsum respectively, during their carbonation. The results confirmed the detection of the beginning of the carbonation and allowed us to identify some consumed and formed chemical phases in the early stages of the reaction. These outcomes of *in situ* Raman spectroscopy monitoring study on cementitious phases could help understand the early chemical modifications occurring in complex environments such as cement pastes.

Keywords

Carbonation, Raman spectroscopy, principal component analysis, ettringite, monosulfoaluminate.

1. Introduction

Carbonation is one of the most common chemical reactions that take place in cementitious materials. Atmospheric CO_2 diffuses into the material through its porous network and reacts with different

* Corresponding author. Email address: mohamed-nadjib.brahim@univ-lorraine.fr / brahim.mohamed.nadjib@gmail.com (M-N.Brahim)

hydrates of the cement paste. Carbonation leads to a decrease of pH value that damages the passivation layer of the concrete steel reinforced bars and may then initiate the corrosion of the bars [1]. This phenomenon concerns both ordinary Portland cement (OPC) [2,3] and calcium sulfoaluminate (CSA) cement [4,5].

In a previous study, Marchetti et al. [6] presented a new method using Raman spectroscopy that enables the early detection of cementitious materials carbonation. This approach was non-destructive and measurements were performed *in situ* at a given depth of the material. These preliminary investigations were solely conducted on portlandite which was chosen to validate the method. In the present study, tests are specifically conducted on the sulfoaluminate hydrates (ettringite and monosulfoaluminate). The objective was to test the feasibility of the detection of the beginning of their carbonation by in-situ Raman spectroscopy and also to investigate the early stages of their reaction. Understanding how to accurately detect carbonation in each of the pure phases (portlandite, ettringite, monosulfoaluminate, calcium silicate hydrate, etc) and the resulting changes using this new method is an essential step to apprehend results of measurements in a complex environment such as ordinary Portland cement or calcium sulfoaluminate cement binders.

CSA cement, which is mainly composed of yeelimite ($C_4A_3\check{S}$ [†]), represents a good opportunity to experimentally produce a large amount of ettringite and/or monosulfoaluminate. Indeed, its main hydrates are aluminium hydroxide (AH_3), ettringite ($C_6A\check{S}_3H_{32}$) and monosulfoaluminate ($C_4A\check{S}H_{12}$) [7]. They are the products of the yeelimite hydration which is often idealized by the reactions (Reac. 1) and (Reac. 2) [7].

$$\underset{\text{(yeelimite)}}{C_4A_3\check{S}} + \underset{\text{(gypsum)}}{2C\check{S}H_2} + \underset{\text{(water)}}{34H} \rightarrow \underset{\text{(ettringite)}}{C_6A\check{S}_3H_{32}} + \underset{\text{(aluminium hydroxide)}}{2AH_3} \quad \text{(Reac. 1)}$$

$$\underset{\text{(yeelimite)}}{C_4A_3\check{S}} + \underset{\text{(water)}}{18H} \rightarrow \underset{\text{(monosulfoaluminate)}}{C_4A\check{S}H_{12}} + \underset{\text{(aluminium hydroxide)}}{2AH_3} \quad \text{(Reac. 2)}$$

Ettringite and monosulfoaluminate, also designated as AFt and SO_4-AFm phases respectively, can also form in the Portland cement paste [8].

These two sulfoaluminate phases can carbonate in presence of CO_2 [4,9] and some hypotheses about the products of these reactions exist in the literature.

[†] Cement notation: C = CaO, A = Al_2O_3, Š = SO_3, H = H_2O, Č = CO_2

It has been reported that ettringite carbonation leads to the formation of calcium carbonate (CC̄), water, gypsum ($C\bar{S}H_2$) and possibly hemihydrate ($C\bar{S}H_{1/2}$), as well as aluminium hydroxide (AH_3) or alumina gel (AH_x) [10–12] according to (Reac. 3) or (Reac. 4) [10,12]. In their ettringite carbonation study, Nishikawa et al. [10] indicated that the polymorph of the calcium carbonate that forms at first is vaterite and that later aragonite becomes the predominant phase. On the other hand, Gastaldi et al. [13] indicated that the three $CaCO_3$ polymorphs are formed.

$$C_6A\bar{S}_3H_{32} + 3\bar{C} \rightarrow 3C\bar{C} + 3C\bar{S}H_2 + AH_x + (26 - x)H \quad \text{(Reac. 3)}$$

$$C_6A\bar{S}_3H_{32} + 3\bar{C} \rightarrow 3C\bar{C} + 3C\bar{S}H_{1/2} + AH_3 + 27.5H \quad \text{(Reac. 4)}$$

During both OPC and CSA cements reactions with CO_2, the carbonation of monosulfoaluminate generates calcium carbonate, aluminium hydroxide, gypsum and water (Reac. 5) [4,14,15]. In the case of anhydrite/yeelimite blends carbonation, Hargis et al. [14] indicated the initial conversion of SO_4-AFm to ettringite and monocarboaluminate ($C_4A\bar{C}H_{11}$) as expressed in (Reac. 6). Monocarboaluminate will then react according to (Reac. 7), and following this, ettringite will carbonate to form CC̄, $C\bar{S}H_2$, AH_3 and water [14]. Depending on the reaction kinetics, it may not be possible to observe the production of this carboaluminate phase and monosulfoaluminate may carbonate directly as indicated in (Reac. 5) [14]. Authors working on this subject have indicated that calcite is the $CaCO_3$ polymorph produced in these reactions.

$$C_4A\bar{S}H_{12} + 3H\bar{C} \rightarrow 3C\bar{C} + AH_3 + C\bar{S}H_2 + 10H \quad \text{(Reac. 5)}$$

$$6C_4A\bar{S}H_{12} + 3H\bar{C} + 25H \rightarrow 2C_6A\bar{S}_3H_{32} + 3C_4A\bar{C}H_{11} + AH_3 \quad \text{(Reac. 6)}$$

$$C_4A\bar{C}H_{11} + 3H\bar{C} \rightarrow 4C\bar{C} + AH_3 + 11H \quad \text{(Reac. 7)}$$

According to Gastaldi et al. [13], calcium carbonate is expected to form instead of monocarboaluminate, in the case of the CSA cement paste carbonation, as follows (4H were added to balance the original chemical equation and were considered as the water produced during carbonation):

$$3C_4A\bar{S}H_{14} + 6\bar{C} \rightarrow C_6A\bar{S}_3H_{32} + 6C\bar{C} + 2AH_3 + 4H \quad \text{(Reac. 8)}$$

When present, monosulfoaluminate is reported in the literature to be among the first hydrates to react as soon as the material is in contact with CO_2. Thermodynamic calculations simulating carbonation using an ordinary cement composition performed by Glasser & Matschei [16] show that monosulfoaluminate decomposes as soon as CO_2 is available. Similarly, Shah et al. [17] noticed from phase assemblages calculations based on an ordinary Portland cement that the first reaction

occurring during carbonation is the conversion of monosulfoaluminate to monocarboaluminate. For CSA cement, Gastaldi et al. [13] reported that monosulfoaluminate was the first phase to carbonate in their cement paste carbonation simulation. Seo et al. [4] investigated the carbonation of CSA cement and concluded the first phases to be carbonated were SO_4-AFm and AFt. This means that, monosulfoaluminate may be the first phase to react in the pristine core zone of the OPC paste when the carbonation front reaches this zone and the same phase with the addition of ettringite may come first in the case of CSA cement paste. Investigating the early stages of these two sulfoaluminate phases carbonation in the absence of any other hydrates submitted to this reaction may thus help to understand the early occurring chemical modifications. Such an approach requires the early detection of the carbonation front arrival at a given depth of the studied material.

Raman spectroscopy is used to obtain information on the chemical composition and structure of a material and to identify substances contained in a studied sample [18,19]. It has been used in some studies for the investigation of cementitious materials carbonation [6,20–23]. Marchetti et al. showed that *in situ* monitoring of carbonation using Raman spectroscopy is possible [6]. This vibrational spectroscopy technique is considered to be non-destructive [24–26]. It offers the possibility of analysing samples without any preparation [19] and through glass containers [19,26] with appropriate transmission value. A Raman spectrum can be acquired in a few minutes or even seconds. During reaction monitoring, setting a short delay between two successive spectra enables the collection of a large data set to improve the odds of accurately detecting any significant and relevant chemical evolutions of the material. Furthermore, sulfate ion SO_4^{2-} is a polyatomic anion that normally gives rise to relative sharp peaks, and so does the carbonate anion [27]. Using this technique is thus relevant to monitor early sulfoaluminate phases carbonation. Many Raman spectra of Portland Cement and CSA cement pastes found in the literature show relatively intense bands attributed to ettringite and/or monosulfoaluminate, including when the paste contains low amounts of these hydrates [28–32]. Specific monitoring of these phases should thus facilitate the detection of their evolutions during the carbonation.

A similar experimental protocol to the one implemented in [6] to detect carbonation front arrival on portlandite with *in situ* Raman monitoring was used in this study to investigate the early stages of the ettringite and monosulfoaluminate carbonation. The approach described in this research is nevertheless significantly more complex because of the presence of several phases, as presented in

the aforementioned reactions, as compared with solely using portlandite [6]. *In situ* Raman monitoring was conducted at nearly 5mm depth of two pastes of hydrated synthetic yeelimite in the presence and absence of gypsum respectively, while exposed to a CO_2-enriched atmosphere. X-ray diffraction (XRD) and thermogravimetric analysis (TGA) measurements were also conducted to support results obtained by Raman spectroscopy. Raman spectra coupled with principal component analysis confirmed the beginning of carbonation and enabled the identification of some of the consumed and formed chemical phases in the early stages of the reaction.

2. Materials and methods

2.1. Raw materials

The experiments were performed using a synthesised yeelimite ($C_4A_3\check{S}$) and a commercial gypsum ($C\check{S}H_2$). For the first experiment, a sample prepared prior to this study by a cement research laboratory was given to the Institut Jean Lamour laboratory (University of Lorraine) for X-ray fluorescence (XRF) analysis. The data provided and the loss of ignition at 950°C are shown in Table 1. The XRD pattern and the Raman spectrum are presented in Figure 1 and Figure 2 respectively. The commercial gypsum ($C\check{S}H_2$) was a calcium sulphate dihydrate AnalaR NORMAPUR® analytical reagent (from VWR). Assay results indicated by the provider are higher than 99.8%. Figure 2 shows its average Raman spectrum.

Table 1 shows that traces of silica are present in the yeelimite sample which could correspond to a small amount of quartz. In the yeelimte X-ray diffractogram, characteristic peaks of the orthorhombic polymorph pattern were observed at around $2\theta = 18°$ and $2\theta = 20.5°$ [33]. Cubic and tetragonal polymorphs may also be present in the sample. Very weak peaks at $2\theta = 25.4°$ and $2\theta = 37.4°$ could be due to traces of anhydrite and lime respectively. Some few weak peaks could not be attributed to any phase.

Figure 2 shows raw spectra without artefacts. Yeelimite has an intense peak at 988 cm^{-1} corresponding to ν_1 $[SO_4]^{2-}$ mode and a weak peak at 611 cm^{-1} attributed to ν_4 $[SO_4]^{2-}$ mode [32,34]. The band that arises from ν_1 $[AlO_4]^{5-}$ vibration may be the band at around 515 cm^{-1} as suggested by Gastaldi et al. [32] or the broad band at around 464 cm^{-1} as reported by Torréns-Martín et al. and Tang et al. [34,35]. In gypsum spectrum, a very strong sharp peak at 1004 cm^{-1} is clearly observed

and is assigned to ν_1 $[SO_4]^{2-}$ mode. The minor peaks at 411 cm^{-1} and 489 cm^{-1} are due to ν_2 $[SO_4]^{2-}$ vibrations, the one at 1133 cm^{-1} to ν_3 $[SO_4]^{2-}$ and the two bands at 615 and 666 cm^{-1} are assigned to ν_4 $[SO_4]^{2-}$ modes [32].

Table 1 Chemical composition (with the statistical error, due to the XRF spectrometer, of the value of each oxide) and loss on ignition of the synthesised yeelimite.

Oxide	CaO	Al_2O_3	SO_3	SiO_2	Fe_2O_3	LOI
% in weght	38.1	48.9	12.1	0.6	0.1	0.81
Statistical error (%)	0.6	1	1.3	9.7	6.0	

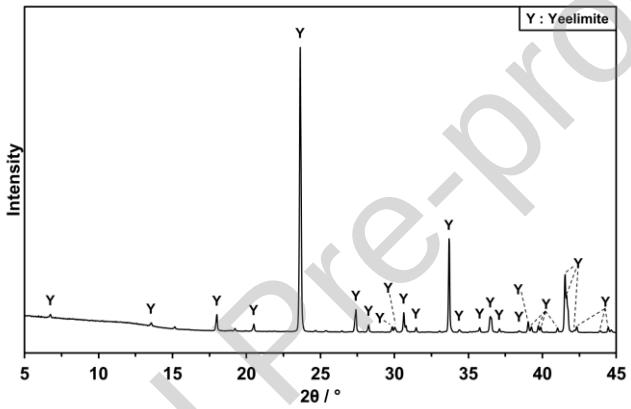

Figure 1 X-ray diffraction pattern of the synthesised yeelimite.

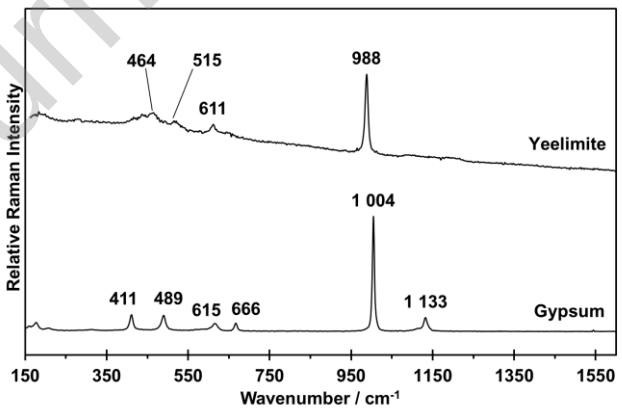

Figure 2 Raman spectra of raw materials yeelimite ($C_4A_3\check{S}$) and commercial gypsum ($C\check{S}H_2$) (average spectrum) (acquired using a B&WTek i-Raman spectrometer, 785 nm laser wavelength, integration time of 30 s).

2.2. Paste preparation and experimental setup description

Two pastes which were respectively mixtures of yeelimite (Y), gypsum (G), water (W), and yeelimite (Y), water (W) were prepared. In the first experiment “Y+G+W”, yeelimite was hydrated in presence of gypsum to form ettringite and aluminium hydroxide (Reac. 1) [7]. Yeelimite and gypsum powders were first mixed together and homogenised before hydration. In the second “Y+W” experiment, only yeelimite was used to form monosulfoaluminate (Reac. 2) [7]. The expected chemical reactions (Reac. 1) and (Reac.2) are given in the introduction.

47g and 38g of paste were prepared with water/cement ratios of 0.64 (experiment 1: "Y+G+W") and 0.58 (experiment 2: "Y+W") respectively. In experiment 1, the correct amounts of reactants were mixed to match with reaction 1 (Reac. 1) stoichiometry. In experiment 2, a 10% excess of water was added to the w/c ratio that satisfies reaction 2 (Reac. 2) stoichiometry to prevent desiccation during the curing step. A ControLab overhead stirrer equipped with a straight-blade impeller was used to prepare the mixes.

The reactors consisted in a plastic bottle equipped with a compression gland at its bottom for each experiment. This gland was used to seal a clear glass vial with the opening outside the plastic bottle, as shown in Figure 3. To avoid using a large amount of yeelimite powder, sand and a two-component epoxy adhesive (ARALDITE® 2020, ideal for bonding glass and ceramics) were poured into the reactors to fill the gap between the bottoms of the plastic bottle and the glass vial. Pastes were poured in after the epoxy resin hardening. The Raman probe could then be inserted into the vial to perform measurements on the paste through the glass. The bottom side of a similar reactor was checked and was waterproof and airtight.

Each reactor was filled with a paste approximately 5 mm thick above the glass vial bottom (Figure 3). Given amounts of each fresh paste were also put in separated small bottles (Ø ≈ 28 mm) for further analysis by XRD and TGA. The pastes poured in the small bottles were few millimetres height. The reactors and the small bottles were then sealed with caps and put in a climate chamber (Memmert ICH 260C) for curing for roughly 30 days. At the end of this curing step, samples were collected from the hardened paste contained in the small bottles to be analysed by means of XRD and TGA. The cap of the reactor was removed while the atmosphere of the chamber was set so as to guarantee a CO_2 concentration of 3% to enhance carbonation. The control accuracy of the CO_2 concentration

indicated by the climate chamber manufacturer is ±0.2%. Experiments were not considered completed before the detection of $CaCO_3$ by means of Raman spectroscopy. Y+G+W and Y+W pastes were left in the chamber for carbonation for approximately 21 days and 8 days respectively. In the case of Y+W, after almost 7 days of carbonation, the CO_2 inlet was closed for 10 days and then set back to 3% for approximately 1 day. We assumed that this interruption has no effect on the carbonation process. During both the curing and carbonation steps of Y+G+W and Y+W, relative humidity and temperature were controlled by the climate chamber and were respectively around 65% and 20°C. A few variations were observed for short durations due to the climate chamber opening or other undetected reasons, and considered to be of no incidence on the pastes. Furthermore, the position of the Raman probe may have changed as we opened the reactor. The zones analysed during the two steps may thus be slightly different, although this is considered as having had no incidence on experimental results.

After the end of the carbonation process of both experiments, the reactors were removed from the climate chamber, visually checked and stored under room environmental conditions. During storage, pastes were kept inside their respective closed reactors. The mineralogy of the analysed zone of the paste is thus unlikely to significantly change. After ~ 1 week and ~ 4 months of storage for Y+G+W and Y+W respectively, a sample from the zone of the paste monitored by Raman spectroscopy was collected to be analysed by XRD and TGA. All TGA in this study were performed under air flow (around 25 ml/min according to laboratory) by setting the heating rate to 10°C/min until reaching around 994°C. XRD measurements were carried out between 6° and 69° (2θ angle) using BRUKER D8 advance and PANalytical X'Pert Pro MPD diffractometers with a Cu K_α radiation at the wavelength of 1.5406 Å. Both diffractometers were working in Bragg-Brentano geometry.

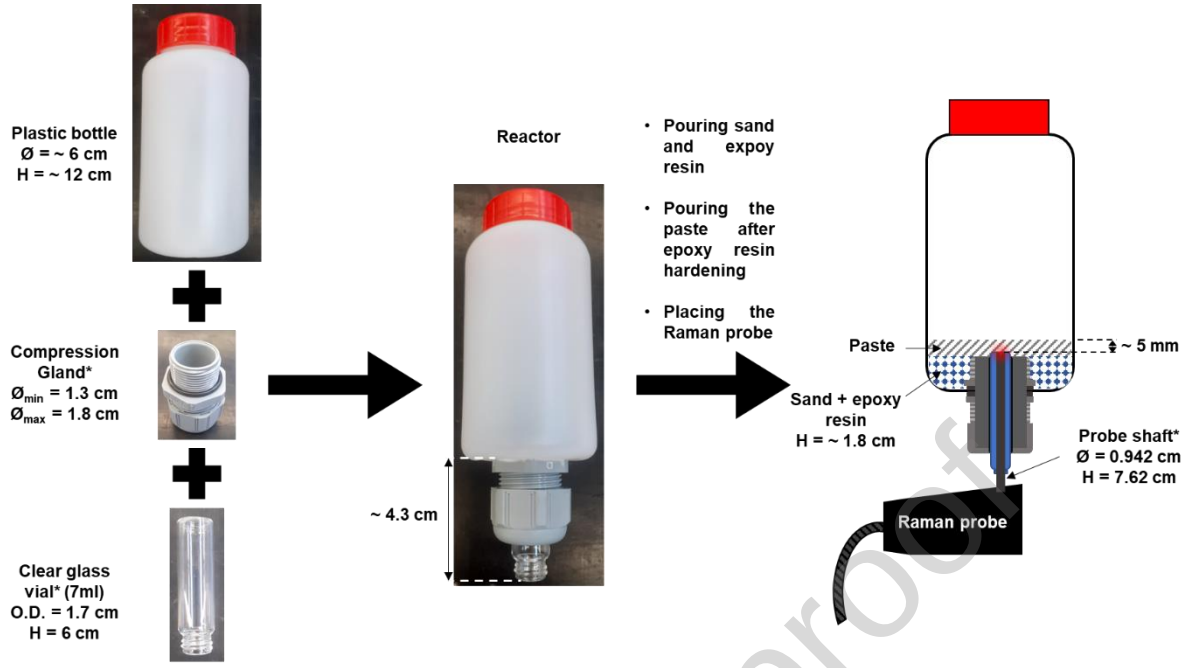

Figure 3 Reactor preparation steps. H = height; O.D. = outer diameter; Ø = diameter (* = values indicated by the manufacturer).

2.3. Raman spectroscopy monitoring

The instrument used was a B&WTek i-Raman® 785S spectrometer, using a 785 nm excitation, equipped with a BAC102 probe. The manufacturer's specifications indicate that the resolution is ~ 4.5 cm^{-1} at 912 nm and that the laser spot diameter at focal plane is around 85 µm. The Raman spectra of the curing and the carbonation steps were acquired over the 150-3200 cm^{-1} spectral range. The whole experiment was performed with the maximum laser power delivered at the end of the probe. It was measured using a laser power meter and was about 60 mW. BWSpec 4.11_1 software was used for the data acquisition and dark subtraction.

The spectroscopic monitoring was performed choosing a time interval between two successive spectra set to five minutes. A single spectrum was measured using three accumulations with one minute exposure time for each to increase the signal intensity. The spectrum is the average of these three accumulations. Averaging reduced noise that can be considered as an experimental error and which could come from different sources (such as the detector of the spectrometer [36]). Furthermore, relative intensities at some Raman shift positions were monitored to detect evolutions in the spectra. The relative intensity is the difference between the absolute intensity value at the considered Raman shift and the ordinate of its projection onto a defined baseline. This baseline was

defined by linking two points, one right before and one right after the peak (or peaks, in case of overlapping bands). The baseline could thus be different from a spectrum to another but for each case, the Raman shifts of these two points were set fixed over time to be able to compare the relative intensities. The relative intensities were calculated from the raw spectra data. This was performed using BWSpec, Microsoft Excel 2019 and OriginPro 9 software with the latter also used for peak area calculations.

2.4. Spectra pre-treatment and principal component analysis

Raman matrices of the curing and the carbonation steps for each experiment (Y+W and Y+G+W) were formed by arranging Raman spectra of each step into rows. Each matrix was then made of intensities values where each row represented a spectrum acquired at a given time and each column represented a specific Raman shift.
Before analysis and interpretation steps, these matrices were pre-treated and selected pre-processing methods are listed below:

Removing spikes and artefacts (RS): Plotting and analysing the raw Raman spectra matrices revealed the presence of spikes and signal artefacts (that can be due to the instrument). Artefacts usually occur at a same wavenumber value in many spectra. The presence of spikes and artefacts induces an inappropriate variance in the spectra, and will influence principal component analysis results. It is therefore necessary to remove them beforehand and was done using VBA codes on Microsoft Excel.

Savitzky-Golay smoothing (SG): This smoothing was performed on each spectrum of the Raman matrices after the previous pre-treatment to reduce the influence of noise on principal component analysis results. The Chemflow project [37] developed in Galaxy was used for this, with a derivative order equal to 0, a size of window equal to 7, and a second degree polynom.

Baseline correction (DT4): This consisted in an orthogonal projection of each spectrum as a detrend onto a 4-order polynom. The aim is to reduce the influence of baseline variation, observed in the spectra, on principal component analysis results. This pre-treatment was performed using Chemflow.

Standard Normal Variate (SNV): This pre-treatment was also performed on Chemflow and transforms the mean and the standard-deviation of each spectrum to 0 and 1 respectively. Like the previous pre-processing method, it helps reduce variation due to the spectra baselines.

Baseline correction (BLcor): This specific pre-treatment was performed when the 1034-1102 cm^{-1} spectral range was analysed alone to reduce the variation of the spectra baselines. An orthogonal projection of spectra onto a straight line was performed. Spectra were then shifted to positive values. Finally, from each spectrum, we subtracted its minimum intensity value.

An accurate detection of evolutions in the Raman matrices of both experiments was eased by using principal component analysis (PCA). PCA is an exploratory chemometric method used to identify any hidden structure into datasets and to reduce the variables dimensionality with the identification of relationships between variables. PCA is meant to elaborate a lower-dimensional space from a large dataset [38], where new directions are orthogonal and along which the variance is maximum. Based on a nonlinear iterative partial least squares (NIPALS) algorithm or on a singular value decomposition (SVD), and the diagonalization of variance-covariance matrix, new variables are built as a linear combination of physical variables but are uncorrelated. PCA decomposes the spectra matrix X as follows [18]:

$$X = SL^T + E$$

in which S is the scores matrix that represents coordinates of each spectrum in the new axes (Principal components), L is the loading matrix and represents the contribution of each of the original variables, i.e., Raman shifts, to build the principal component. E is the residue matrix that could be related to measurement noise.

A statistical approximation will replace the physics, and the chemistry ruling observed phenomena is partly hidden. New directions in this space, or loadings, do contain the underlying physical and chemical information. Furthermore, a dispersion of datapoints (i.e., change in coordinates) into a direction given by a loading does imply an evolution of the chemical of the corresponding principal component. Each datapoint (spectrum) was timestamped so that the kinetics of the evolution was available.

PCA was performed using Chemflow on the Raman matrices after pre-treatment to detect any evolutions as early as possible and to identify the evolving peaks. Variables (i.e., column of intensities of each Raman shift) were centred but not scaled, and the number of PCs for each analysis

was chosen at its maximum value, i.e., 20. Table 2 indicates the pre-treatment types performed on all the Raman spectra displayed in this paper. It also indicates the spectra population and the spectral range to which pre-treatment and PCA were applied.

Table 2 Characteristics of pre-treatments and PCA performed on Raman spectra (of carbonation step) of the displayed results in this paper.

Experiment	Figure	Pre-treatment			PCA (if applicable)	
		Type (in order)	Spectral range (cm^{-1})	Raman spectra population	Spectral Range (cm^{-1})	Raman spectra population
Y+G+W (carbonation step)	Figure 5a	RS	150-3200	1392 first		
		RS SG	150-1700			
	Figure 7a	RS	150-3200	1392 first		
		RS SG SNV	150-1700			
	Figure 8	RS	150-3200	1392 first	150-1200	1000 first
		RS SG SNV	150-1700			
		DT4	150-1200	1000 first		
	Figure 11	(Same as Figure 8)			150-1200	150^{th} to 350^{th}
Y+W (carbonation	Figure 5b	RS SG	150-1700	1217 first		

step)						
	Figure 7b	RS SG SNV	150-1700	1217 first		
	Figure 9	RS SG DT4	150-1700	1217 first	150-1200	1217 first
		SNV	150-1200	1217 first		
	Figure 13	(Same as Figure 9)			1020-1140	1217 first

3. Results and discussion

3.1. The end of the curing step

Figure 4 shows XRD and TGA results performed on pastes of both experiments at the end of the curing step.

For Y+G+W, XRD shows ettringite and gypsum patterns along with the presence of yeelimite. The weak peak around 2θ = 10° was assigned in some studies using CSA cement or yeelimite/gypsum system pastes to monosulfoaluminate (SO_4-AFm) [7,39] but was attributed in others to ettringite (AFt) [13,40]. At the same time, the derivative curve (DTG) did not exhibit a well-defined weight loss at around 190°C that could correspond to monosulfoaluminate decomposition. Although ettringite is the main sulfoaluminate hydrate formed, it may not be the only one. A small amount of monosulfoaluminate may have also formed despite the yeelimite by gypsum ratio chosen while preparing the paste. Furthermore, TGA data indicates weight losses at around 145°C and 280°C that were attributed to ettringite and to gibbsite (AH_3) decompositions respectively [41]. Both XRD and TGA show the absence of calcium carbonate in the sample even though it was collected from the air-contact surface of the paste. The mass loss observed at around 100°C in the DTG curve may be due to the amorphous aluminium hydroxide decomposition [39] or to free water evaporation. TGA

results did not clearly indicate gypsum dehydration. Ettringite decomposition between approximately 100-200 °C may hinder its observation.

For Y+W, ettringite, monosulfoaluminate with two different hydration states ($C_4A\check{S}H_{12}$ and $C_4A\check{S}H_{14}$, noted M12 and M14 respectively in the XRD pattern of Figure 4) and the unhydrated yeelimite were detected by XRD in the sample. The Y+W TGA data displayed in the Figure 4 are the results of the analysis performed on a paste prepared following a similar experimental protocol as that for the preparation of the paste used for the Raman monitoring. It was stored for ~ 30 days in a room where the temperature was set to 20°C and the relative humidity was not controlled. The same peaks are present in the XRD patterns performed on this paste and on the paste prepared for Raman monitoring with some intensities differences. The main difference is the intensity of the $C_4A\check{S}H_{14}$ pattern. It was higher in the paste prepared for Raman monitoring. Y+W TGA results confirm the formation of monosulfoaluminate (weight loss at around 200°C) and aluminium hydroxide (weight loss at around 275°C) [42,43]. Weight losses at temperatures below 170°C are due to $C_4A\check{S}H_{12}$ and ettringite decomposition [42,43]. They can also be attributed to the dehydrations of $C_4A\check{S}H_{14}$ [42] and the amorphous aluminium hydroxide. The very small weight loss (Δm = 0.6%) observed at around 700°C suggests the presence of traces of calcium carbonate in the sample. The sample was taken from the air-contact surface. This surface could have started carbonating during the curing step leading to the formation of calcium carbonate. Furthermore, in the diffractograms, some few weak peaks could not be attributed to any phase.

In addition, in PCA performed on the last 800 Raman spectra of both the Y+G+W and Y+W experiments before setting CO_2 concentration to 3% in the ambient air, none of the PCs that showed evolution indicated the presence of a calcium carbonate peak (around 1085 cm^{-1} [22,44]). In the last 800 Raman spectra (corresponding to approximately 5 days) of Y+G+W curing step, only a very small decrease (< 1.7%) in the trend of the relative intensities of the peak at 986 cm^{-1} attributed to ettringite (see Table 3) was observed. This intensity decrease could have been due to ettringite dehydration because the laser may have locally heated the material. Ettringite is among the first phases to decompose when a CSA cement paste is analysed by TGA [7]. However, since this Raman intensity decrease is very small, the possible laser-induced heating could be neglected and Y+G+W and Y+W experiments can be considered to be non-destructive. Furthermore, peaks monitoring

indicated that the relative intensities of the ν_1; ν_2; ν_3 and ν_4 $[SO_4]^{2-}$ peaks due to gypsum (see Table 3) were increasing in Y+G+W spectra. The reason of this increase is unknown.

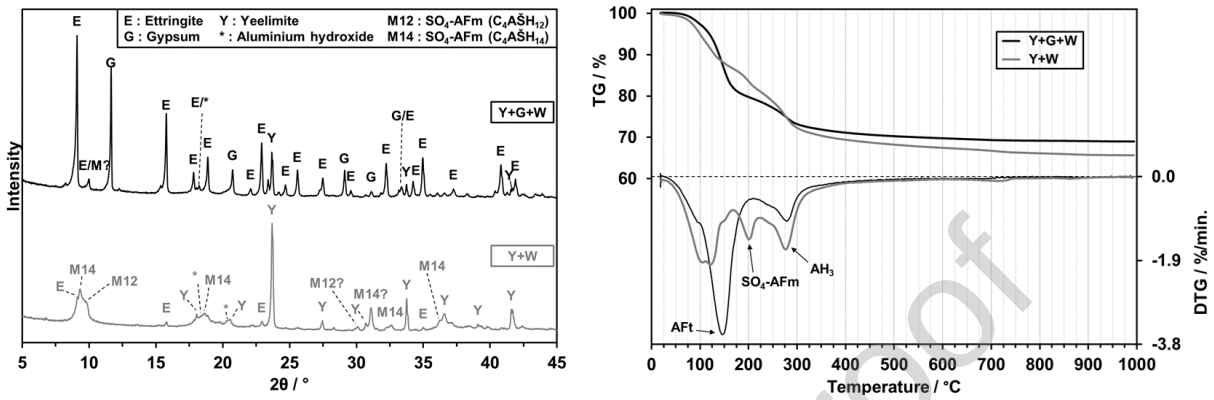

Figure 4 Results of XRD (left) and TGA (right) performed on the samples collected at the end of the curing step for Y+G+W (black lines) and Y+W (grey lines).

The first Raman spectra acquired during the carbonation step are shown in Figure 5. Table 3 gives the band positions and their potential corresponding assignments (vibrations and phases). After the end of the curing step, the Raman probe may have been moved while opening the reactor thus slightly modifying the analysed zone. Figure 5 shows also the last spectrum of the curing step. The Figure indicates that peaks remained at the same positions or close after opening the reactors. However, the relative intensities of some bands changed. This difference could be only due to the amount of the detected phases present in the zones analysed before and after the reactors opening.

Figure 5a shows that gypsum was clearly detected in the Y+G+W paste, which is consistent with XRD results. The same bands in the spectrum obtained from gypsum alone were observed: at 1004 cm^{-1} (ν_1 $[SO_4]^{2-}$), at 1133 cm^{-1} (ν_3 $[SO_4]^{2-}$), at 411 and 489 cm^{-1} (ν_2 $[SO_4]^{2-}$) and at 615 and 668 cm^{-1} (ν_4 $[SO_4]^{2-}$). The sharp peak that appears at 984 cm^{-1} and the weak bands at 449 cm^{-1} and 538 cm^{-1} are respectively attributed to ettringite ν_1 $[SO_4]^{2-}$, ν_2 $[SO_4]^{2-}$ and Al-(OH) stretching vibration modes. These two phases share the same peak at 615 cm^{-1} corresponding to the same vibration mode (ν_4 $[SO_4]^{2-}$). The weak shoulder at 1112 cm^{-1} can also be considered to be a peak shared by these two phases. It was assigned to ν_3 $[SO_4]^{2-}$ [32,34,40,45–48]. The unreacted yeelimite could have also been detected. If this is the case, the peaks at 984 cm^{-1} (ν_1 $[SO_4]^{2-}$), 615 cm^{-1} (ν_4 $[SO_4]^{2-}$) would be a mixture of ettringite and yeelimite signals and also gypsum in the case of 615 cm^{-1}.

In the Y+W spectrum (Figure 5b), a sharp peak appears at 525 cm^{-1} unlike in the other experiment. This is unlikely to be the Al-(OH) stretching band of ettringite. In fact, the latter emerges at a slightly different wavenumber and is much weaker as can be seen in Y+G+W spectrum and as has been reported in the literature [34,40]. The same applies to the ν_1 $[AlO_4]^{5-}$ vibration band of yeelimite (see Figure 2). We also assumed that it cannot be attributed to calcium aluminate hydrates either, since none of these phases was observed in the XRD pattern. This peak was thus assumed to correspond to the Al-(OH) stretching of monosulfoaluminate [34,40] in its both hydration states $C_4AŠH_{12}$ and $C_4AŠH_{14}$, as reported in the literature [34,49]. Peaks at 986 cm^{-1}, 440 cm^{-1} and 608 cm^{-1} are most probably a mixture of monosulfoaluminate [34,40,49], ettringite and the unreacted yeelimite signals. The broad bands at 460 cm^{-1} and at ~1100 cm^{-1} could be respectively due to the ν_2 $[SO_4]^{2-}$ vibration of yeelimite [35] and the ν_3 $[SO_4]^{2-}$ vibration of monosulfoaluminate and/or ettringite [40].

Besides that, the absence of the monosulfoaluminate characteristic peak at 525 cm^{-1} in the Y+G+W spectrum is noteworthy. However, this does not necessarily mean that this phase is absent in the analysed zone. A small amount of this phase could have formed and its signal may have been weak enough to only generate the ν_1 $[SO_4]^{2-}$ band at around 985 cm^{-1}. In this case, its 985 cm^{-1} peak could have been added to the mixture of ettringite and yeelimite signals. Furthermore, aluminium hydroxide and calcium carbonate peaks are absent in both spectra. The broad bands at ~ 1150-1700 cm^{-1} in both spectra were due to the glass vial because this band appeared when the raw materials were analysed using the vial. The vial also generates a large weak band at ~ 230-520 cm^{-1}. Moreover, we could not attribute the weak peak at 313 cm^{-1} and the broad band at ~730-870 cm^{-1} to any phase.

The calcium aluminate hydrates CAH_{10}, C_2AH_8 and C_4AH_{13} may potentially form during yeelimite hydration [50,51] but none of these phases were detected in our both XRD patterns. Torrens et al. [34,52] reported that C_2AH_8 and C_4AH_{13} could generate some Raman bands but mainly in the O-H stretching region (> 3400 cm^{-1}) which is beyond the spectral range covered by our spectrometer. They also indicated that weak peaks appear at 334 cm^{-1} and 357 cm^{-1} in the C_4AH_{13} spectrum. These two bands were not observed in our spectra.

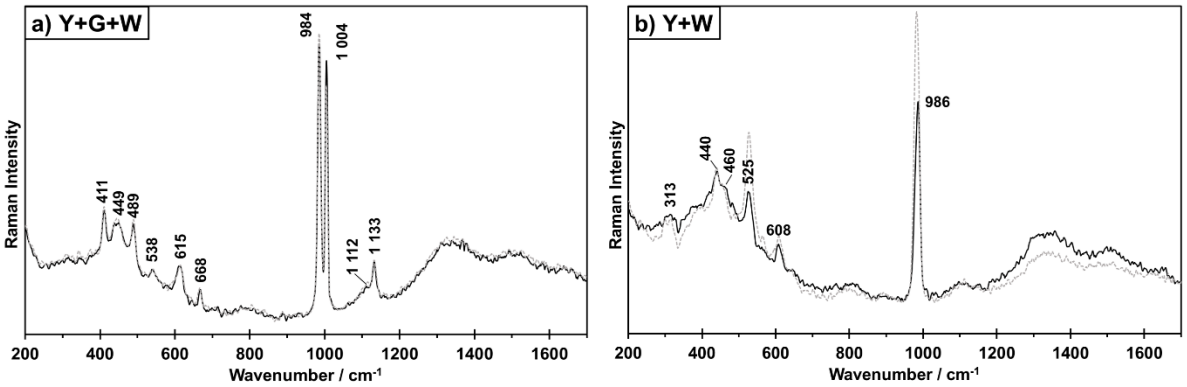

Figure 5 First Raman spectrum (black line) of the carbonation step and last Raman spectrum (dashed grey line) of the curing step for each experiment (after RS then SG pre-treatments).

Table 3 Assignments of the identified peaks in the first Raman spectrum of the carbonation step for each experiment. vw = very weak; w = weak; m = medium; vs = very strong; b = broad.

Experiment	Band position (cm^{-1})	Assignment	Possible corresponding phases	Reference
Y+G+W	1133 w	ν_3 $[SO_4]^{2-}$	Gypsum	[32,45,46]
	1004 vs	ν_1 $[SO_4]^{2-}$		
	668 vw	ν_4 $[SO_4]^{2-}$		
	411 w	ν_2 $[SO_4]^{2-}$		
	489 w	ν_2 $[SO_4]^{2-}$		
	615 w	ν_4 $[SO_4]^{2-}$	Gypsum / Ettringite / Yeelimite	[32,34,40,45]
	1112 vw	ν_3 $[SO_4]^{2-}$	Ettringite / Gypsum	[40,45–47]
	984 vs	ν_1 $[SO_4]^{2-}$	Ettringite / Yeelimite	[32,34,47,48]
	538 vw	Al-(OH) stretch	Ettringite	[34,47]
	449 w	ν_2 $[SO_4]^{2-}$		
Y+W	~1100 b	ν_3 $[SO_4]^{2}$	Monosulfoaluminate / Ettringite	[40,49]

440 w	ν_2 $[SO_4]^{2-}$		
986 vs	ν_1 $[SO_4]^{2-}$	Monosulfoaluminate / Ettringite /	[34,40,49]
608 w	ν_4 $[SO_4]^{2-}$	Yeelimite	
525 m	$Al(OH)_6$ stretch	Monosulfoaluminate	[34,40]
460 b	ν_2 $[SO_4]^{2-}$	Yeelimite	[35]

3.2. The carbonation step

Figure 6 shows XRD and TG analysis performed on samples collected from both Y+G+W and Y+W pastes from the zones where Raman measurements were conducted after the end of the carbonation step. The results obtained suggest that the carbonation front reached the analysed zone because they show presence of calcium carbonate. Aragonite polymorph was detected in both samples. Vaterite was only detected in the Y+W paste. The results also indicate that sulfoaluminate hydrates reacted.

For Y+G+W, only traces of ettringite were detected by XRD while the gypsum pattern is clearly visible but the intensity of the most intense peak of gypsum did not increase compared to the one in the diffractogram obtained at the end of the curing step. Furthermore, the two peaks observed in DTG near 150°C and 170°C are due to gypsum ($C\check{S}H_2$) and hemihydrate ($C\check{S}H_{1/2}$) dehydrations. Despite the identification of gypsum by XRD and TGA, both techniques do not clearly indicate its formation during carbonation. The weak peaks of hemihydrate visible in the Y+G+W XRD pattern confirm that this phase was formed during carbonation. Ndiaye et al. [12] also detected this phase among the products that formed after ettringite decomposition under 4% CO_2 concentration. However, in the present study, an XRD analysis was performed on the paste of a small bottle taken out from the carbonation chamber at ~ 4 days after setting CO_2 concentration to 3%. The samples analysed were collected at 0-3 mm and 3-5 mm depths and the results did not show any presence of hemihydrate. This phase certainly formed later on during the reaction (after the first four days). Moreover, in TGA, the weight loss at ~ 100°C observed in Figure 6 corresponds to the evaporation of free water and may also be due the amorphous aluminium hydroxide dehydrations.

For Y+W, monosulfoaluminate was not detected by XRD, and DTG did not clearly show the peak at 200°C corresponding to its dehydration. This suggests that this phase has been totally carbonated. However, the Y+W XRD pattern did reveal the presence of ettringite even after over 8 days of carbonation. The ettringite detected could have already been formed during the curing step and not carbonated at that point and/or a neo-formed ettringite. In TGA, weight losses at around 130°C were most probably due to ettringite. The XRD and TGA results did not clearly indicate the presence of gypsum in the sample. In the Raman spectra, intensities at some wavenumbers in the 1000 – 1025 cm^{-1} spectral range were randomly changing during the curing and the carbonation steps. This poor signal to noise ratio did not allow a clear identification of a possible gypsum formation (ν_1 $[SO_4]^{2-}$ gypsum peak expected around 1005 cm^{-1}). This artefact was therefore removed to avoid any influence on Principal Component Analysis results. Moreover, the strong peak at 2θ = ~ 22.5° could not be assigned to any phase and was probably due to some impurities that may have been unintentionally added to the sample.

As for the results obtained at the end of the curing step, the remaining yeelimite and aluminium hydroxide were clearly detected by XRD and TGA (weight losses near 275°C) respectively in both experiments (Figure 6). Also in the diffractograms, some few weak peaks could not be attributed to any phase.

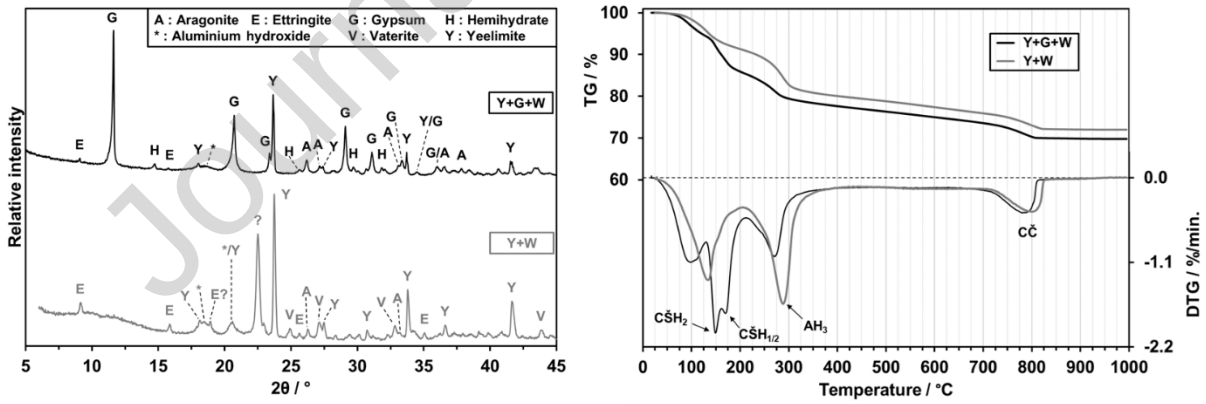

Figure 6 Results of XRD (left) and TGA (right) performed on the samples collected after the end of the carbonation step for Y+G+W (black lines) and Y+W (grey lines); (? : unidentified peak).

In the Y+G+W experiment, the first 1392 Raman spectra collected during the carbonation step (nearly 8 days of carbonation) were pre-treated and analysed. In the Y+W experiment, the first 1217 spectra (corresponding to almost 7 days) of the carbonation step were studied.

Figure 7 shows Raman spectra acquired after around one hour, and one to four days and almost one week after CO_2 was set to 3%. Some evolutions were observed in the Y+G+W spectra (Figure 7a). On almost the 7th day, the intensities of the peaks at ~ 984 cm^{-1} and ~ 445 cm^{-1} decreased corresponding to ettringite decomposition, as observed in XRD results. The peak at around 1004 cm^{-1} increased due to calcium sulfate formation. Furthermore, a new peak is observed at ~ 1082 cm^{-1}, attributed to calcium carbonate formation. These evolutions are consistent with the carbonation reaction (Reac. 3). In the Y+W experiment (Figure 7b), over the first ~ 7 days, apart from the small increase of the band at around 1060-1100 cm^{-1} and the slight decrease of the ~525 cm^{-1} peak, no other visible change was observed.

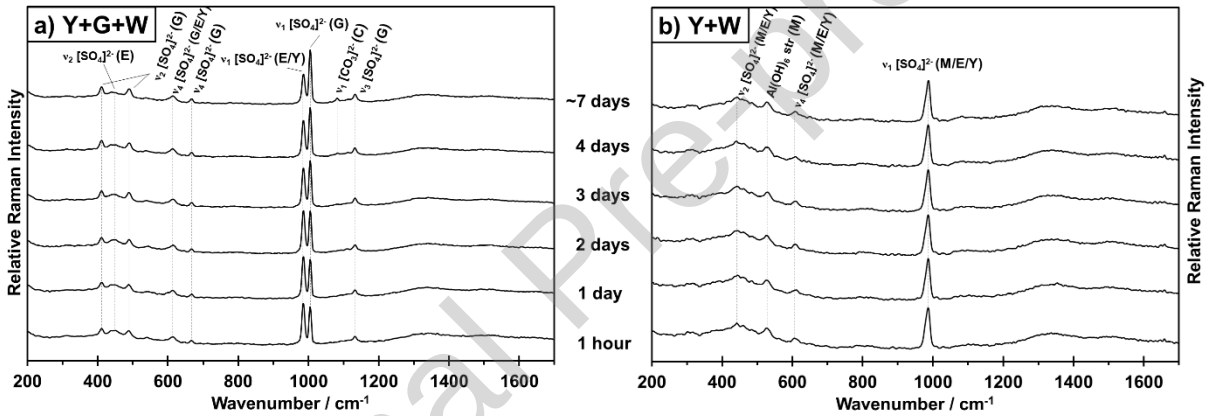

Figure 7 Y+G+W and Y+W Raman spectra at different times of the carbonation step. E : ettringite, G : gypsum, M : monosulfoaluminate, Y : yeelimite, C : calcium carbonate.

To investigate the beginning of carbonation reaction and accurately detect the front arrival, PCA was performed on the Raman spectra corresponding to the carbonation step occurring in both experiments. The results are presented in Figure 8 (Y+G+W) and Figure 9 (Y+W). Only PC1 and PC2 that explain nearly 92% and 4% of the variance in Y+G+W and around 43% and almost 8% of the variance in Y+W respectively were considered. PC coordinates changes do indicate chemical evolutions in both cases. A significant and sudden change occurred at around 20 hours (~ 150th spectrum) in the case of Y+G+W, while, a decreasing trend from the beginning was observed in PC1 with strong fluctuations in both coordinates in the case of Y+W.

Concerning the other components, in analysis related to the Y+G+W case PC4 and PC5 that explain ~0.32% and ~0.15% of the variance respectively show little variation but not a clear evolution. In

addition, their loadings either show contributions at the same Raman shift positions as that observed in the first two principal components or closer or alternatively information considered to be irrelevant that could be assimilated with noise contribution. The same observation was carried out on the fourth PC (explained variance: 3.04%) of the PCA performed on the spectra obtained in the case of Y+W. All the other PC's coordinates of both PCA fluctuated around 0 and were attributed to spikes that were not properly corrected or noise.

The change observed in PC1 and PC2 coordinates in the case of Y+G+W carbonation indicates that the analysed zone evolved. Marchetti et al. [6] performed similar investigations which were limited to Portlandite however. They stated that a sudden change in PC coordinates may be assimilated to the beginning of the studied zone carbonation. Based on that, and on the PCA performed on the 100 first spectra that did not show any evolution, the sudden PC coordinates change at ~ 20 hours (~ 150th spectrum) in the case of Y+G+W was assumed to correspond to the starting point of the carbonation reaction. Loadings indicate that the variation in the pre-treated spectra is mainly due to the peaks corresponding to gypsum pattern (1004; 411; 492; 1133; 617; 666 cm^{-1}), to ettringite pattern (984; 440/443/454; 545 cm^{-1}) and to calcium carbonate (1082 cm^{-1}). Yeelimite may also be among the phases that contribute to this variation. However, the ettringite reaction hindered its observation as peaks generated by ν_1 and ν_4 $[SO_4]^{2-}$ vibrations and the band at around 450 cm^{-1} of these two phases do emerge at close wavenumbers. Furthermore, despite the absence of the peak at 525 cm^{-1}, monosulfoaluminate may also slightly contribute to variance with only the ν_1 $[SO_4]^{2-}$ band if its signal is too weak, as explained earlier.

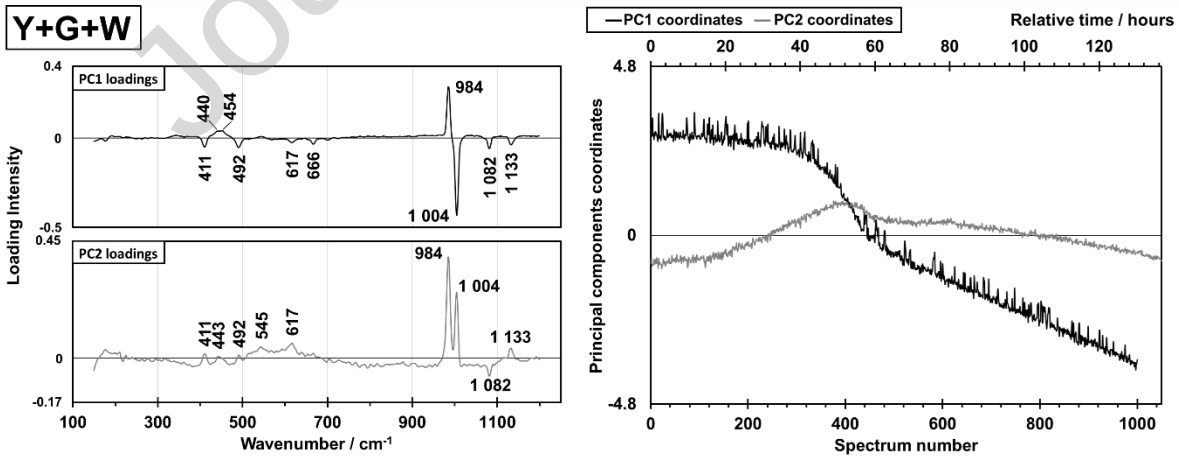

Figure 8 Loadings (left) and coordinates (right) of PC1 and PC2 of the PCA performed on the 1000 first spectra of Y+G+W carbonation step.

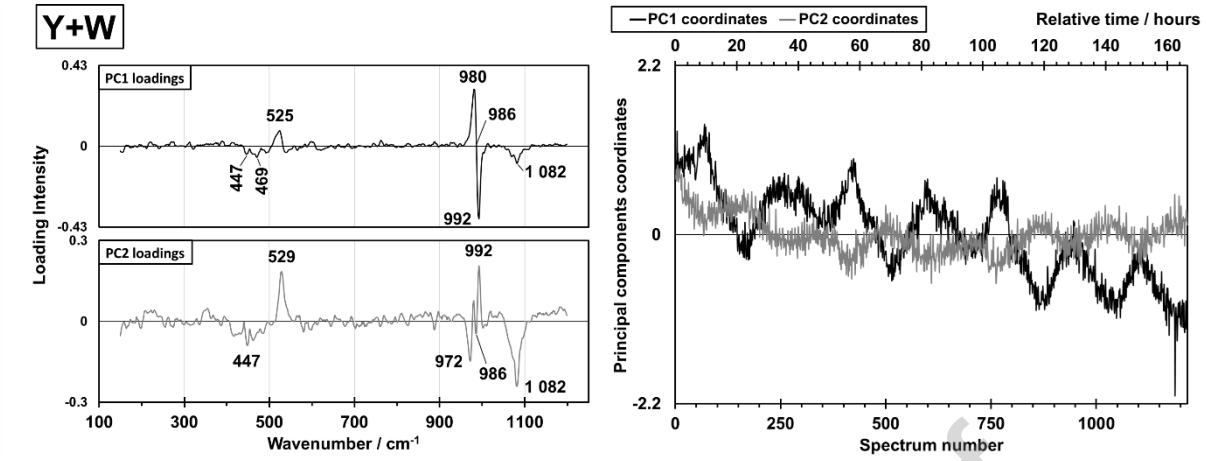

Figure 9 Loadings (left) and coordinates (right) of PC1 and PC2 of the PCA performed on the 1217 first spectra of Y+W carbonation step.

Interpreting the results of the PCA performed on the Raman matrix in the case of Y+W was more complex. The contribution of the intensities at 986 cm^{-1} to the variation in the spectra seems to be very low whereas those closer at 980 cm^{-1} and 992 cm^{-1} represent the highest contributions in PC1. Peak monitoring (Figure 10b) indicated that the intensity at 980 cm^{-1} was decreasing while the one at 992 cm^{-1} started slowly increasing from roughly the 900th spectrum (after around 5 days of carbonation) and the 986 cm^{-1} slightly decreased. This means that the shape of the peak at 986 cm^{-1} was changing without a significant evolution of the peak top intensity. As explained previously, this peak is likely to be a mixture of signals of ettringite, monosulfoaluminate and the unreacted yeelimite. Variations at both 992 cm^{-1} and 980 cm^{-1} could thus be respectively due to the formation of ettringite and to the monosulfoaluminate carbonation with the first being a result of the second in accordance to (Reac. 6) or (Reac. 8). The literature tells us that the highest Raman peak in ettringite spectrum does not always emerge at the same wavenumber as the one in the monosulfoaluminate spectrum [35,40,49]. The late increase of the intensity at 992 cm^{-1} could be related to the kinetics of ettringite precipitation. The amount of ettringite that could have formed is low which may explain why no significant difference of the peaks intensity was observed in the diffractograms of the curing and the carbonation steps. In addition to that, the possible hydration of the yeelimite reacting with water released from carbonation occurring close to the analysed zone could also contribute to the variation of this Raman peak. Likewise, weak peaks in the range 440-480 cm^{-1} could originate from one carbonation-induced variation or a mixture of these. In this way, they could be attributed to ν_2 $[SO_4]^{2-}$ of ettringite that could have been forming, ν_2 $[SO_4]^{2-}$ of monosulfoaluminate that was carbonating and ν_1 $[AlO_4]^{5-}$ of yeelimite that could have been hydrating. Furthermore, the monitoring

of the relative intensities at 992 cm^{-1} during both the curing and the carbonation steps showed similar fluctuations to those observed in the PCA performed on the 150-1200 cm^{-1} spectral range. The reason for this observation could be the weak resolution (~ 4.5 cm^{-1}) and sensitivity of the spectrometer which was thus unable to distinguish the peaks that emerge at close Raman shifts. Moreover, a different shape of the 980 cm^{-1} intensity evolution over time was noticed when the peak monitoring was performed on pre-treated spectra. Pre-treatment may have an effect on Raman spectra. The SG smoothing, for instance, may lead to a loss of information if the size window chosen is large [18]. To avoid any influence due to pre-treatment, all the peaks monitoring presented in this paper were performed on raw spectra. However for PCA, pre-treatment was necessary to reduce the influence of baseline variations, noise, spikes and artefacts. Besides that, the 972 cm^{-1} wavenumber contributes to the PC2 variation (Figure 9). Martinez-Ramirez et al. [53] observed a band at 972 cm^{-1} in the spectrum of a hydrated white cement and attributed it to ν_3 $[SO_4]^{2-}$ vibration of the sulfoaluminate phases. In our study, this peak could not be attributed to any phase.

PCA on spectra in the case of Y+W revealed presence of the peak at 1082 cm^{-1} attributed to ν_1 $[CO_3]^{2-}$ vibration mode of calcium carbonate. This peak was not clearly visible in spectra but as it contributed a great deal to the variation, it clearly appeared in the loadings thus indicating the relevance and the interest of PCA. It also revealed the contribution of the 525/529 cm^{-1} peak that is most probably due to monosulfoaluminate decomposition.

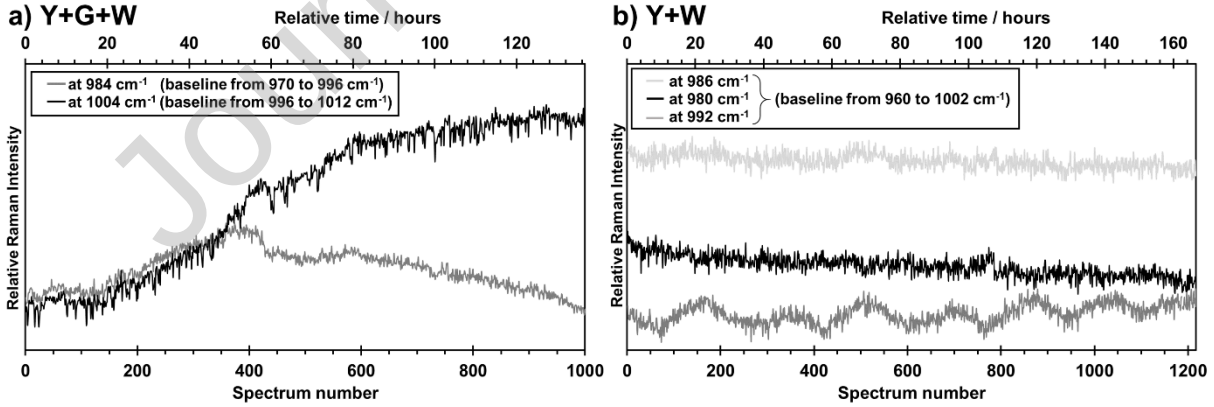

Figure 10 Monitoring of relative intensities at 985 cm^{-1} and 1005 cm^{-1} for Y+G+W and 980 cm^{-1}, 986 cm^{-1} and 992 cm^{-1} for Y+W during carbonation step (A spike was removed from the 992 cm^{-1} relative intensity curve).

The strong bands at 985 cm^{-1} and 1005 cm^{-1} observed in the case of Y+G+W were monitored during the carbonation step and their relative intensities versus time are presented in Figure 10a. In both

cases, the relative intensity suddenly starts to increase at around the 150th spectrum, indicating a starting point of chemical evolution. This observation is consistent with what was obtained from PCA. In addition, areas of these two peaks in the 150th, 200th, 250th, 300th and 350th spectra were checked and were also increasing. The relative intensity of the peak at 1005 cm^{-1} then kept increasing while its counterpart at 985 cm^{-1} started decreasing from approximately the 400th spectrum (at ~ 54 hours). The 1005 cm^{-1} peak is a priori due to ν_1 $[SO_4]^{2-}$ vibration of gypsum. Results of the PCA performed on the 150th to 350th spectra (i.e. approximately 20 to 47 hours) show that PC1 coordinates are increasing (Figure 11). Analysis of its loadings indicates that, besides 1082 cm^{-1}, 988 cm^{-1} and 447 cm^{-1} contributions, the evolution could also be due to peaks at the same or very similar positions of peaks that could be attributed to the ν_1 $[SO_4]^{2-}$(at 1006 cm^{-1}), ν_2 $[SO_4]^{2-}$(at 411 et 494 cm^{-1}), ν_3 $[SO_4]^{2-}$(at 1133 cm^{-1}) and ν_4 $[SO_4]^{2-}$(at 617 et 668 cm^{-1}) vibration mode of gypsum. The relative intensity monitoring of all these peaks attributed a priori to gypsum showed that they all have the same evolution. However, since XRD did not clearly indicate gypsum formation during carbonation, the increase of the intensity of these peaks (at 1006; 411; 494; 1133; 617 and 668 cm^{-1}) at the beginning of the carbonation step was attributed to the formation of a poorly crystalline or amorphous calcium sulfate as most probably a product of carbonation. they cannot be attributed to hemihydrate because of the absence of its pattern in the diffractogram of the sample analysed after 4 days of carbonation. Wang et al. 2012 [54] showed that amorphous calcium sulfate (ACS) and hemihydrate can be sequentially precipitated prior to gypsum formation. Raman bands generated by the poorly crystalline or amorphous calcium sulfate may emerge at the same or similar Raman shifts to those that are due to gypsum. Wang et al. 2022 [55] attributed a sulfate band at 1002 cm^{-1} to the ν_1 $[SO_4]^{2-}$ vibrations of ACS. Furthermore, the other principal components of the PCA performed on the 150th to 350th spectra do not indicate any information considered relevant.

On the other hand, ettringite formation is likely to be the reason for the 985 cm^{-1} relative intensity increase from approximately the 150th to 350th spectra. It is unlikely to be due to monosulfoaluminate formation resulting from yeelimite hydration, as the band around 525 cm^{-1} does not appear among the PC1 loading peaks of the PCA presented in Figure 11 while the weaker band generated by ν_2 $[SO_4]^{2-}$ vibration of AFt/ SO_4-AFm phases does appear (at 447 cm^{-1}). For the same reason, the ettringite formation is unlikely to be the result of the monosulfoaluminate carbonation. It is more likely to be a product of the yeelimite hydration with the water that was released from carbonation occurring close to the analysed zone. The evolutions are consistent with those observed during the beginning of the curing step in the case of Y+G+W. During the beginning of the curing step, the

peaks at around 984 cm^{-1} and 445 cm^{-1} were seen to be increasing, corresponding to the ettringite formation. For the same reason once again, the calcium sulfate formation is unlikely to be due to monosulfoaluminate carbonation. It is most probably a product of ettringite carbonation. As the literature does not indicate any carbonation reaction of a certain phase that produces ettringite and calcium sulfate at the same time, these evolutions most probably mean that (Reac. 1) and (Reac. 3) (with probably poorly crystalline or amorphous calcium sulfate produced instead of gypsum) occur simultaneously in the analysed zone. Finally, beyond the 400th spectrum, the amount of ettringite that is decomposing seems to be greater than the amount forming because of a decreasing relative intensity of 984 cm^{-1} peak.

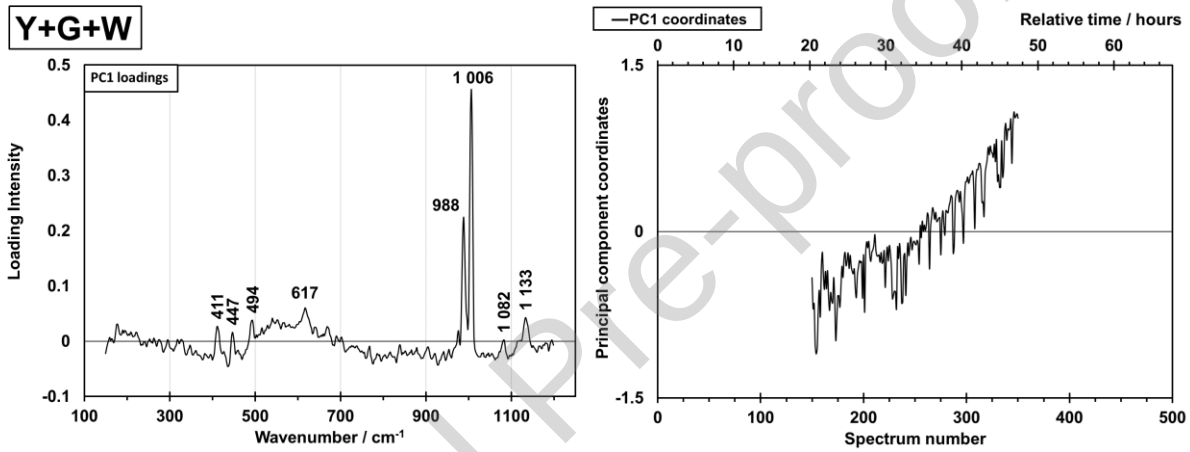

Figure 11 Loadings (left) and coordinates (right) of PC1 of the PCA performed on the spectra from the 150th to the 350th of the Y+G+W carbonation step.

The starting point of the 1082 cm^{-1} peak emergence and increase during the carbonation of Y+G+W was identified at around the 300th spectrum (at ~ 40 hours) in its relative intensity monitoring (Figure 12a). None of the other Raman shift in the 1060-1100 cm^{-1} spectral range, in which the ν_1 $[CO_3]^{2-}$ band of the carbonate-bearing phases that could form appear [27], showed an earlier beginning of evolution. This starting point was thus considered to originate from the ν_1 $[CO_3]^{2-}$ band formation attributed to calcium carbonate (calcite and/or aragonite) [27]. Furthermore, the evolution of the peak shows a weak shoulder on the low Raman shift side which means the formation of the band at 1082 cm^{-1} may be accompanied by the formation of the ν_1 $[CO_3]^{2-}$ band of another carbonate-bearing phase, probably amorphous calcium carbonate (at ~1077 cm^{-1} [27]).

The reason for the time lag between the 1005 cm^{-1} peak increase and the 1082 cm^{-1} band formation is unknown although it may be related to the kinetics of calcium carbonate and calcium sulfate

precipitation. Further experimental work is needed to clarify what happens between the moment the carbonation front arrived and the formation of the 1082 cm^{-1} peak.

Since the loadings of Figure 9 show a large band in the region where the ν_1 $[CO_3]^{2-}$ peak of the carbonate-bearing phases that could form appear, a PCA was performed on the 1020-1140 cm^{-1} spectral range of the Y+W carbonation spectra (Figure 13) to identify the beginning of evolution in this range. Results show that evolution in this range starts from the very beginning of CO_2 injection. The PC1 loading clearly shows the high contribution of the 1082 cm^{-1} wavenumber that corresponds to ν_1 $[CO_3]^{2-}$ band indicating the calcium carbonate formation (calcite and/or aragonite). The relative intensity monitoring confirmed that the peak at 1082 cm^{-1} formed and started increasing from the beginning of the carbonation step (Figure 12b). Loadings also show significant contributions at closer wavenumbers indicating that other peaks closer to the one at 1082 cm^{-1} were forming. This is induced by the ν_1 $[CO_3]^{2-}$ band of the vaterite polymorph (at ~ 1090 cm^{-1} and ~1074 cm^{-1} [27,56]) and probably by the ν_1 $[CO_3]^{2-}$ band of amorphous calcium carbonate and/or carboaluminate phases (~1064 cm^{-1} [27]). If a carboaluminate phase was formed, it could have been transformed before the end of the carbonation step which would explain the absence of its pattern in Y+W Diffractogram (Figure 6).

In the Y+W spectra, the evolution of the peak at 525 cm^{-1} also began very early after CO_2 injection (Figure 14). Its intensity decreased which indicates the monosulfoaluminate carbonation. Moreover, the fact that calcium sulfate was not detected, the early calcium carbonate formation and the possible formation of ettringite indicate that monosulfoaluminate most probably carbonates according to (Reac. 8) from the beginning.

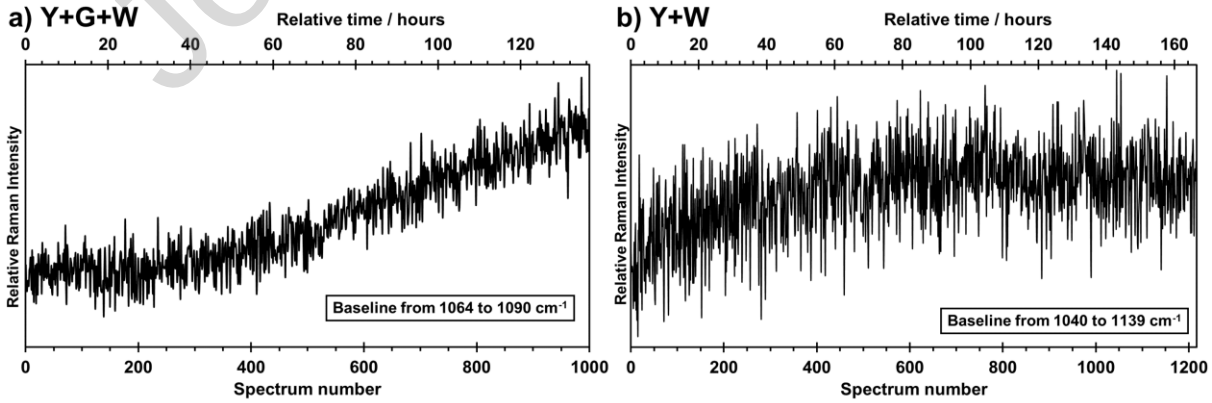

Figure 12 Monitoring of relative intensities at 1082 cm^{-1} in (a) Y+G+W spectra and (b) Y+W spectra during carbonation step.

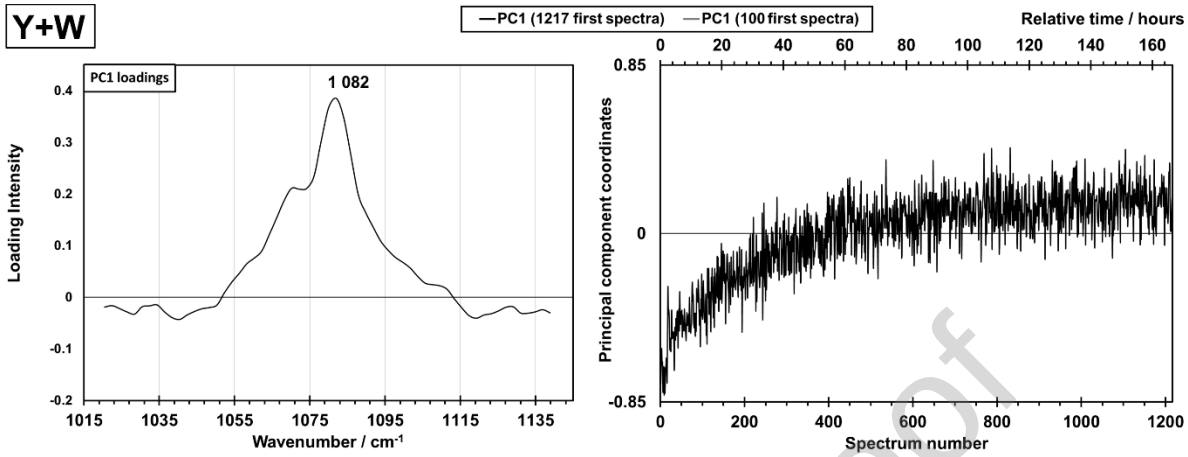

Figure 13 Loadings and coordinates of PC1 of the PCA performed on the 1217 first spectra (black line) and 100 first spectra (grey line) of the Y+W carbonation step, both on the range 1020-1140 cm^{-1}.

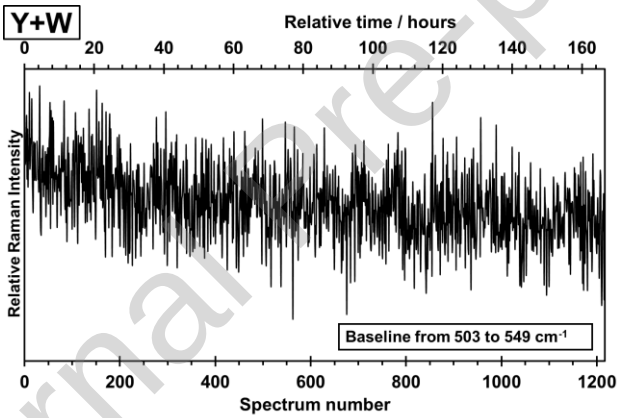

Figure 14 Monitoring of relative intensities at 525 cm^{-1} in Y+W spectra during carbonation step (some spikes were removed).

The starting points of the first chemical evolutions and the very likely reasons for these are summarised in Table 4. The influence of noise and fluctuations due a priori to spectral resolution of the instrument prevented a more accurate detection based on PCA results and peak monitoring. The carbonation reaction occurs much earlier in the case of Y+W than for Y+G+W. The rapid carbonation of the hydrated yeelimite is likely to be due to the reactor used in Y+W experiment. This reactor may have not been as airtight as expected and atmospheric CO_2 may have passed into it and reacted with material located in the Raman-analysed zone before the front arrival. In fact, traces of the paste were found on the Raman probe at the end of Y+W carbonation step indicating that when the paste was fresh it flowed out of the reactor perhaps because the compression gland was not correctly closed.

Finally, PCA enabled the detection of the beginning of evolution in a certain spectral range but did not enable to decompose the mix of chemical reactions hidden in the data. The principal components are not spectra of pure phases [18] but are assimilated to these. An unmixing resolution tool such as Multivariate Curve Resolution - Alternating Least Squares (MCR-ALS) may be more appropriate to decompose the Raman matrix into pure phase spectra and their concentration profiles. However, this is not possible if these pure phases have the same spectra or correlated concentration profiles [18].

Table 4 Summary of the starting points of first chemical evolutions and the highly reasons for these in the carbonation step of both experiments.

Experiments	Indicators of the beginning of carbonation (significant evolutions)	Highly likely reasons	At which spectrum it started to occur?	Corresponding time (after CO_2 injection)
Y+G+W	Sudden PC2 coordinates evolution in the 1000 first spectra PCA	Carbonation front arrival	~ 150^{th}	~ 20 hours
	Increase of the ν_1 $[SO_4]^{2-}$ band at 985 cm^{-1} (peak monitoring)	Ettringite forming from yeelimite hydration	~ 150^{th}	~ 20 hours
	Increase of the ν_1 $[SO_4]^{2-}$ band at 1005 cm^{-1} (peak monitoring)	Calcium sulfate formation from ettringite carbonation	~ 150^{th}	~ 20 hours
	PC1 coordinates evolution in the PCA performed on the 1034-1102 cm^{-1} spectral range	Calcium carbonate (ν_1 $[CO_3]^{2-}$) forming from ettringite carbonation	~ 300^{th}	~ 40 hours

Y+W	PC1 coordinates evolution in the PCA performed on the 1020-1140 cm^{-1} spectral range	Calcium carbonate (ν_1 $[CO_3]^{2-}$) formation from monosulfoaluminate carbonation	These indicators of Y+W seem to indicate the beginning of carbonation very early after CO_2 injection	
	Decrease of the $Al(OH)_6$ stretching band at 525 cm^{-1} (peak monitoring)	Monosulfoaluminate carbonation		
	Decrease of the ν_1 $[SO_4]^{2-}$ band at 980 cm^{-1} (peak monitoring)	Monosulfoaluminate carbonation		
	Increase of the ν_1 $[SO_4]^{2-}$ band at 992 cm^{-1} (peak monitoring)	Ettringite formation	Around the 900^{th}	Around 5 days

4. Conclusion

This study demonstrates that the in situ Raman monitoring enables the accurate detection of the beginning of the sulfoaluminate phases' carbonation. It also helps investigate the early stages of their reaction. Raman spectroscopy effectively detects ettringite and monosulfoaluminate and some of their carbonation products like calcium sulfate and calcium carbonate. This vibrational technique is non-destructive and is therefore an appropriate tool to monitor their carbonation.

During the carbonation of the paste prepared from yeelimite, gypsum and water, in which ettringite was the main sulfoaluminate hydrate formed, the carbonation front arrival was characterised by the increase in the Raman patterns intensity of calcium sulfate and ettringite. This suggests the occurrence of two reactions simultaneously. The first is the carbonation of ettringite and the second a complementary hydration of yeelimite with the water that was probably released from carbonation occurring close to the analysed zone. A few hours after the front detection, evolutions due to the first reaction were the only ones observed. The peak at 1082 cm^{-1}, attributed to calcium carbonate, emerged a little later than the carbonation front arrival. Further investigations are required to identify the reason for this time lag (may be by TGA and Scanning electron microscopy investigation at different moments in the early stages of the reaction). Aragonite seems to be the only crystalline phase of $CaCO_3$ formed during ettringite carbonation. The calcium sulfate formed during carbonation was only detected by Raman spectroscopy. It was not detected by XRD because it is poorly crystalline or amorphous and its formation could not be revealed by TGA either because gypsum dehydration was hindered by that of ettringite in the thermogram obtained at the end of the curing step.

In the case of the paste prepared with yeelimite alone in which both ettringite and monosulfoaluminate were formed, the beginning of carbonation was characterised by the formation of the peak at 1082 cm^{-1}, the decrease of the one at 525 cm^{-1} as well as the intensity at 980 cm^{-1}. These three evolutions seemed to start at approximately the same moment. The first is due to calcium carbonate formation and the last two to monosulfoaluminate carbonation. Furthermore, the late increase of the intensity at 992 cm^{-1} was assumed to be due to the late ettringite precipitation. The band at 1064 cm^{-1} which may be due to monocarboaluminate formation could have also been formed. Further experiments are required to confirm the formation of these last two phases (may be by XRD

and Scanning electron microscopy investigation at different ages). The bands at ~ 1090 cm^{-1} and ~ 1074 cm^{-1} corresponding to vaterite are among the peaks formed.

PCA was very useful as an exploratory tool for the analysis of the spectra collected and enabled us to obtain an overview of the evolutions occurring in the Raman spectra. It revealed the data structure, with the starting point of evolution and the small variations that were not immediately observable in the spectra. PCA also highlighted the existence of some overlapping peaks such as those at 980 cm^{-1} and 992 cm^{-1} in Y+W spectra, which appeared to be only one peak at 986 cm^{-1} in the spectra, thanks to their different respective evolutions. Peaks were then monitored to check evolutions in specific Raman shifts.

Finally, the outcomes of this study could be very useful to find out how to use Raman spectroscopy to accurately detect the carbonation front arrival in both a CSA cement and an OPC binders. The sulfoaluminate phases could be among the first phases of these cements to react when the material is made in contact with CO_2. Further studies of the carbonation of these types of cement using *in situ* Raman monitoring would enhance understanding of the early chemical modifications that occur. In addition, a 2-D scale Raman mapping may help to better visualise the carbonation front arrival at a given depth of the paste.

Acknowledgements

The authors would like to express their thanks to the École Européenne d'Ingénieurs en Génie des Matériaux, Nancy, France for providing the Raman spectrometer and especially Professor Isabelle Royaud and Aurélien Richy, an engineering assistant. The authors would also like to thank Romain Trauchessec, Lionel Aranda, Sébastien Cahen, the CCXGamma team, IUT Nancy-Brabois GCCD technicians (Université de Lorraine) and The FM2D team (Université Gustave Eiffel) for their help in the experimental work.

References

[1] A. Poursaee, Corrosion of Steel in Concrete Structures, Elsevier Science, 2016. http://univ.scholarvox.com.bases-doc.univ-lorraine.fr/catalog/book/docid/88832101 (accessed January 3, 2022).

[2] F.S. Fulton, P.H. Crawford, Cement and Concrete, ASTM International, 1974.

[3] B. Šavija, M. Luković, Carbonation of cement paste: Understanding, challenges, and opportunities, Constr. Build. Mater. 117 (2016) 285–301. https://doi.org/10.1016/j.conbuildmat.2016.04.138.

[4] J. Seo, S. Kim, S. Park, H.N. Yoon, H.K. Lee, Carbonation of calcium sulfoaluminate cement blended with blast furnace slag, Cem. Concr. Compos. 118 (2021) 103918. https://doi.org/10.1016/j.cemconcomp.2020.103918.

[5] J.-M. Mechling, A. Lecomte, A. Roux, B. Le Rolland, Sulfoaluminate cement behaviours in carbon dioxide, warm and moist environments, Adv. Cem. Res. 26 (2014) 52–61. https://doi.org/10.1680/adcr.12.00070.

[6] M. Marchetti, J.-M. Mechling, C. Diliberto, M.-N. Brahim, R. Trauchessec, A. Lecomte, P. Bourson, Portable quantitative confocal Raman spectroscopy: Non-destructive approach of the carbonation chemistry and kinetics, Cem. Concr. Res. 139 (2021) 8. https://doi.org/10.1016/j.cemconres.2020.106280.

[7] F. Winnefeld, B. Lothenbach, Hydration of calcium sulfoaluminate cements — Experimental findings and thermodynamic modelling, Cem. Concr. Res. 40 (2010) 1239–1247. https://doi.org/10.1016/j.cemconres.2009.08.014.

[8] K.L. Scrivener, P. Juilland, P.J.M. Monteiro, Advances in understanding hydration of Portland cement, Cem. Concr. Res. 78 (2015) 38–56. https://doi.org/10.1016/j.cemconres.2015.05.025.

[9] Z. Shi, B. Lothenbach, M.R. Geiker, J. Kaufmann, A. Leemann, S. Ferreiro, J. Skibsted, Experimental studies and thermodynamic modeling of the carbonation of Portland cement, metakaolin and limestone mortars, Cem. Concr. Res. 88 (2016) 60–72. https://doi.org/10.1016/j.cemconres.2016.06.006.

[10] T. Nishikawa, K. Suzuki, S. Ito, K. Sato, T. Takebe, Decomposition of synthesized ettringite by carbonation, Cem. Concr. Res. 22 (1992) 6–14. https://doi.org/10.1016/0008-8846(92)90130-N.

[11] Q. Zhou, F.P. Glasser, Kinetics and mechanism of the carbonation of ettringite, Adv. Cem. Res. 12 (2000) 131–136. https://doi.org/10.1680/adcr.2000.12.3.131.

[12] K. Ndiaye, M. Cyr, S. Ginestet, Durability and stability of an ettringite-based material for thermal energy storage at low temperature, Cem. Concr. Res. 99 (2017) 106–115. https://doi.org/10.1016/j.cemconres.2017.05.001.

[13] D. Gastaldi, F. Bertola, F. Canonico, L. Buzzi, S. Mutke, S. Irico, G. Paul, L. Marchese, E. Boccaleri, A chemical/mineralogical investigation of the behavior of sulfoaluminate binders submitted to accelerated carbonation, Cem. Concr. Res. 109 (2018) 30–41. https://doi.org/10.1016/j.cemconres.2018.04.006.

[14] C.W. Hargis, B. Lothenbach, C.J. Müller, F. Winnefeld, Carbonation of calcium sulfoaluminate mortars, Cem. Concr. Compos. 80 (2017) 123–134. https://doi.org/10.1016/j.cemconcomp.2017.03.003.

[15] H. Justnes, J. Skocek, T.A. Østnor, C.J. Engelsen, O. Skjølsvold, Microstructural changes of hydrated cement blended with fly ash upon carbonation, Cem. Concr. Res. 137 (2020) 106192. https://doi.org/10.1016/j.cemconres.2020.106192.

[16] T. Matschei, F.P. Glasser, Interactions between Portland cement and carbon dioxide, in: Montreal, Canada, 2007.

[17] V. Shah, K. Scrivener, B. Bhattacharjee, S. Bishnoi, Changes in microstructure characteristics of cement paste on carbonation, Cem. Concr. Res. 109 (2018) 184–197. https://doi.org/10.1016/j.cemconres.2018.04.016.

[18] Groupe Français de Spectroscopie Vibrationnelle, Spectroscopies vibrationnelles, Éditions des archives contemporaines, 2020.

[19] E. Smith, G. Dent, Modern spectroscopy: a practical approach, Wiley, Chichester, 2005.

[20] J. Bensted, Uses of Raman Spectroscopy in Cement Chemistry, J. Am. Ceram. Soc. 59 (1976) 140–143. https://doi.org/10.1111/j.1151-2916.1976.tb09451.x.
[21] L. Black, C. Breen, J. Yarwood, K. Garbev, P. Stemmermann, B. Gasharova, Structural Features of C–S–H(I) and Its Carbonation in Air—A Raman Spectroscopic Study. Part II: Carbonated Phases, J. Am. Ceram. Soc. 90 (2007) 908–917. https://doi.org/10.1111/j.1551-2916.2006.01429.x.
[22] Y. Yue, J.J. Wang, P.A.M. Basheer, J.J. Boland, Y. Bai, A Raman spectroscopy based optical fibre system for detecting carbonation profile of cementitious materials, Sens. Actuators B Chem. 257 (2018) 635–649. https://doi.org/10.1016/j.snb.2017.10.160.
[23] T. Mi, Y. Li, W. Liu, W. Li, W. Long, Z. Dong, Q. Gong, F. Xing, Y. Wang, Quantitative evaluation of cement paste carbonation using Raman spectroscopy, Npj Mater. Degrad. 5 (2021) 1–7. https://doi.org/10.1038/s41529-021-00181-6.
[24] N. Garg, K. Wang, S.W. Martin, A Raman spectroscopic study of the evolution of sulfates and hydroxides in cement–fly ash pastes, Cem. Concr. Res. 53 (2013) 91–103. https://doi.org/10.1016/j.cemconres.2013.06.009.
[25] F. Haque, R.M. Santos, Y.W. Chiang, Using nondestructive techniques in mineral carbonation for understanding reaction fundamentals, Powder Technol. 357 (2019) 134–148. https://doi.org/10.1016/j.powtec.2019.08.089.
[26] Metrohm, B&W Tek Portable Raman Analyzers, (n.d.). https://www.metrohm.com/en-gb/products-overview/spectroscopy/bw-tek-spectroscopy/bw-tek-portable-raman/ (accessed November 11, 2021).
[27] L. Black, Raman spectroscopy of cementitious materials, in: J. Yarwood, R. Douthwaite, S. Duckett (Eds.), Spectrosc. Prop. Inorg. Organomet. Compd., Royal Society of Chemistry, Cambridge, 2009: pp. 72–127. https://doi.org/10.1039/b715000h.
[28] K. Zhang, M. Yio, H. Wong, N. Buenfeld, Real-time monitoring of carbonation of hardened cement pastes using Raman microscopy, J. Microsc. n/a (2022). https://doi.org/10.1111/jmi.13084.
[29] H.-C. Loh, H.-J. Kim, F.-J. Ulm, A. Masic, Time-Space-Resolved Chemical Deconvolution of Cementitious Colloidal Systems Using Raman Spectroscopy, Langmuir. 37 (2021) 7019–7031. https://doi.org/10.1021/acs.langmuir.1c00609.
[30] Y. Yue, J.J. Wang, P.A.M. Basheer, Y. Bai, In-situ monitoring of early hydration of clinker and Portland cement with optical fiber excitation Raman spectroscopy, Cem. Concr. Compos. (2020) 103664. https://doi.org/10.1016/j.cemconcomp.2020.103664.
[31] M. Torres-Carrasco, A. del Campo, M.A. de la Rubia, E. Reyes, A. Moragues, J.F. Fernández, In situ full view of the Portland cement hydration by confocal Raman microscopy, J. Raman Spectrosc. 50 (2019) 720–730. https://doi.org/10.1002/jrs.5574.
[32] D. Gastaldi, E. Boccaleri, F. Canonico, M. Bianchi, The use of Raman spectroscopy as a versatile characterization tool for calcium sulphoaluminate cements: a compositional and hydration study, J. Mater. Sci. 42 (2007) 8426–8432. https://doi.org/10.1007/s10853-007-1790-8.
[33] J. Zhao, J. Huang, C. Yu, C. Cui, J. Chang, Phosphorus Substitution Preference in Ye'elimite: Experiments and Density Functional Theory Simulations, Materials. 14 (2021) 5874. https://doi.org/10.3390/ma14195874.
[34] D. Torréns-Martín, L. Fernández-Carrasco, S. Martínez-Ramírez, J. Ibáñez, L. Artús, T. Matschei, Raman Spectroscopy of Anhydrous and Hydrated Calcium Aluminates and Sulfoaluminates, J. Am. Ceram. Soc. 96 (2013) 3589–3595. https://doi.org/10.1111/jace.12535.
[35] S.W. Tang, X.H. Cai, W. Zhou, H.Y. Shao, Z. He, Z.J. Li, W.M. Ji, E. Chen, In-situ and continuous monitoring of pore evolution of calcium sulfoaluminate cement at early age by electrical impedance measurement, Constr. Build. Mater. 117 (2016) 8–19. https://doi.org/10.1016/j.conbuildmat.2016.04.096.
[36] P.M. Ramos, I. Ruisánchez, Noise and background removal in Raman spectra of ancient pigments using wavelet transform, J. Raman Spectrosc. 36 (2005) 848–856. https://doi.org/10.1002/jrs.1370.
[37] Galaxy, (n.d.). https://vm-chemflow-francegrille.eu/ (accessed March 1, 2022).
[38] I.T. Jolliffe, Principal Component Analysis, 2nd ed., Springer-Verlag, New York, 2002. https://doi.org/10.1007/b98835.

[39] F. Bullerjahn, J. Skocek, M. Ben Haha, K. Scrivener, Chemical shrinkage of ye'elimite with and without gypsum addition, Constr. Build. Mater. 200 (2019) 770–780. https://doi.org/10.1016/j.conbuildmat.2018.12.170.
[40] G. Renaudin, R. Segni, D. Mentel, J.-M. Nedelec, F. Leroux, C. Taviot-Gueho, A Raman Study of the Sulfated Cement Hydrates: Ettringite and Monosulfoaluminate, J. Adv. Concr. Technol. 5 (2007) 299–312. https://doi.org/10.3151/jact.5.299.
[41] R. Trauchessec, J.-M. Mechling, A. Lecomte, A. Roux, B. Le Rolland, Impact of anhydrite proportion in a calcium sulfoaluminate cement and Portland cement blend, Adv. Cem. Res. 26 (2014) 325–333. https://doi.org/10.1680/adcr.13.00051.
[42] L.G. Baquerizo, T. Matschei, K.L. Scrivener, M. Saeidpour, A. Thorell, L. Wadsö, Methods to determine hydration states of minerals and cement hydrates, Cem. Concr. Res. 65 (2014) 85–95. https://doi.org/10.1016/j.cemconres.2014.07.009.
[43] C.W. Hargis, A. Telesca, P.J.M. Monteiro, Calcium sulfoaluminate (Ye'elimite) hydration in the presence of gypsum, calcite, and vaterite, Cem. Concr. Res. 65 (2014) 15–20. https://doi.org/10.1016/j.cemconres.2014.07.004.
[44] R. Frech, E.C. Wang, J.B. Bates, The i.r. and Raman spectra of CaCO3 (aragonite), Spectrochim. Acta Part Mol. Spectrosc. 36 (1980) 915–919. https://doi.org/10.1016/0584-8539(80)80044-4.
[45] T. Schmid, R. Jungnickel, P. Dariz, Insights into the CaSO4–H2O System: A Raman-Spectroscopic Study, Minerals. 10 (2020) 115. https://doi.org/10.3390/min10020115.
[46] B.J. Berenblut, P. Dawson, G.R. Wilkinson, A comparison of the Raman spectra of anhydrite (CaSO4) and gypsum (CaSO4).2H2O), Spectrochim. Acta Part Mol. Spectrosc. 29 (1973) 29–36. https://doi.org/10.1016/0584-8539(73)80005-4.
[47] S.K. Deb, M.H. Manghnani, K. Ross, R.A. Livingston, P.J.M. Monteiro, Raman scattering and X-ray diffraction study of the thermal decomposition of an ettringite-group crystal, Phys. Chem. Miner. 30 (2003) 31–38. https://doi.org/10.1007/s00269-002-0279-x.
[48] S. Sahu, D.L. Exline, M.P. Nelson, Identification of thaumasite in concrete by Raman chemical imaging, Cem. Concr. Compos. 24 (2002) 347–350. https://doi.org/10.1016/S0958-9465(01)00086-5.
[49] L. Black, C. Breen, J. Yarwood, C.-S. Deng, J. Phipps, G. Maitland, Hydration of tricalcium aluminate (C 3 A) in the presence and absence of gypsum —studied by Raman spectroscopy and X-ray diffraction, J. Mater. Chem. 16 (2006) 1263–1272. https://doi.org/10.1039/B509904H.
[50] F. Bullerjahn, E. Boehm-Courjault, M. Zajac, M. Ben Haha, K. Scrivener, Hydration reactions and stages of clinker composed mainly of stoichiometric ye'elimite, Cem. Concr. Res. 116 (2019) 120–133. https://doi.org/10.1016/j.cemconres.2018.10.023.
[51] F. Winnefeld, B. Lothenbach, Phase equilibria in the system $Ca_4Al_6O_{12}SO_4$ – Ca_2SiO_4 – $CaSO_4$ – H_2O referring to the hydration of calcium sulfoaluminate cements, RILEM Tech. Lett. 1 (2016) 10–16. https://doi.org/10.21809/rilemtechlett.2016.5.
[52] D. Torréns-Martín, L. Fernández-Carrasco, S. Martínez-Ramírez, Hydration of calcium aluminates and calcium sulfoaluminate studied by Raman spectroscopy, Cem. Concr. Res. 47 (2013) 43–50. https://doi.org/10.1016/j.cemconres.2013.01.015.
[53] S. Martinez-Ramirez, M. Frías, C. Domingo, Micro-Raman spectroscopy in white portland cement hydration: long-term study at room temperature, J. Raman Spectrosc. 37 (2006) 555–561. https://doi.org/10.1002/jrs.1428.
[54] Y.-W. Wang, Y.-Y. Kim, H.K. Christenson, F.C. Meldrum, A new precipitation pathway for calcium sulfate dihydrate (gypsum) via amorphous and hemihydrate intermediates, Chem Commun. 48 (2012) 504–506. https://doi.org/10.1039/C1CC14210K.
[55] M. Wang, L. Ji, S. Niu, J. Yang, B. Tang, J. Ni, C. Shao, X. Zhang, X. Yang, Fiber arrangement endow compression resistance of the mantis shrimp hammer-like appendage, J. Mater. Res. Technol. 21 (2022) 3169–3180. https://doi.org/10.1016/j.jmrt.2022.10.112.
[56] C. Gabrielli, R. Jaouhari, S. Joiret, G. Maurin, In situ Raman spectroscopy applied to electrochemical scaling. Determination of the structure of vaterite, J. Raman Spectrosc. 31 (2000) 497–501. https://doi.org/10.1002/1097-4555(200006)31:6<497::AID-JRS563>3.0.CO;2-9.

CRediT authorship contribution statement

Mohamed-Nadjib BRAHIM : Conceptualization, Methodology, Software, Validation, Formal analysis, Investigation, Data curation, Writing – original draft, Writing – review & editing, Visualization, Supervision, Project administration.

Jean-Michel MECHLING : Conceptualization, Methodology, Validation, Formal analysis, Investigation, Data curation, Writing – review & editing, Visualization, Supervision, Project administration.

Mario MARCHETTI : Conceptualization, Methodology, Software, Validation, Formal analysis, Investigation, Writing – review & editing, Visualization, Supervision, Project administration.

Sarah JANVIER-BADOSA : Formal analysis, Writing – review & editing.

Declaration of interests

☒The authors declare that they have no known competing financial interests or personal relationships that could have appeared to influence the work reported in this paper.

☐The authors declare the following financial interests/personal relationships which may be considered as potential competing interests:

Graphical abstract

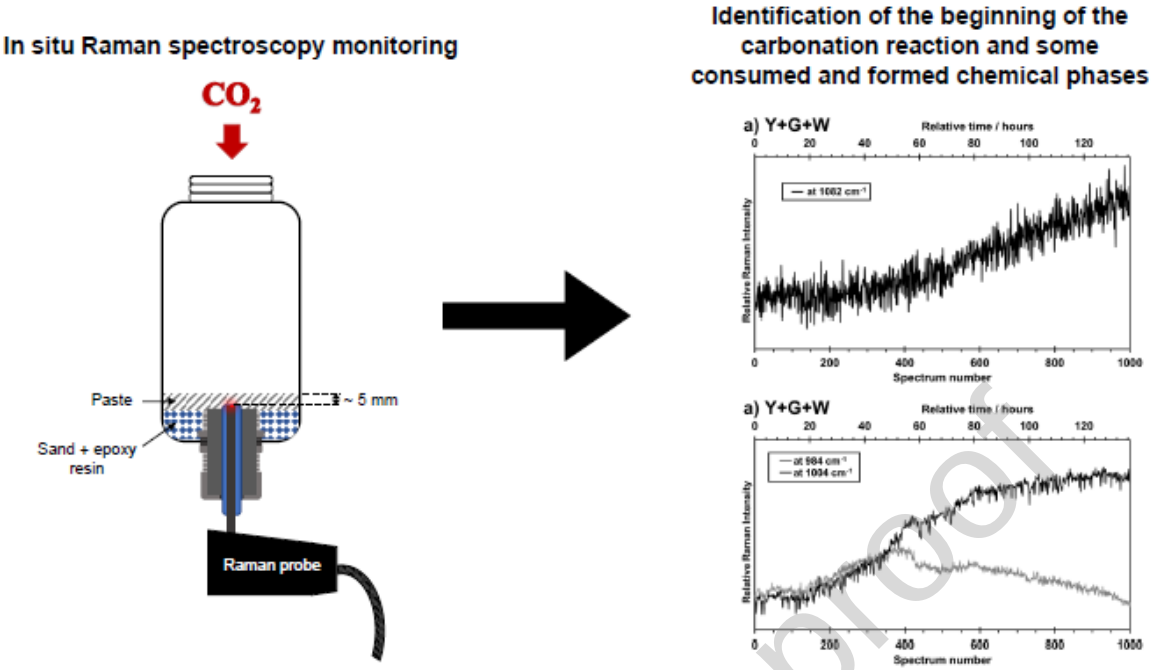

Highlights

- Ettringite and monosulfoaluminate carbonation was monitored by Raman spectroscopy
- The probe inserted at a given depth of the material allowed an *in situ* monitoring
- Raman spectroscopy coupled with chemometrics confirmed the beginning of carbonation
- The evolution of some phases during carbonation was detected by Raman spectroscopy